Schmidt number effects in dissipative particle dynamics simulation of polymers

Vasileios Symeonidis[a] and George Em Karniadakis
Division of Applied Mathematics, Brown University, Providence, Rhode Island 02912

Bruce Caswell
Division of Engineering, Brown University, Providence, Rhode Island 02912

(Received 16 May 2006; accepted 13 September 2006; published online 9 November 2006)

Simulation studies for dilute polymeric systems are presented using the dissipative particle dynamics method. By employing two different thermostats, the velocity-Verlet and Lowe's scheme, we show that the Schmidt number (S_c) of the solvent strongly affects nonequilibrium polymeric quantities. The fractional extension of wormlike chains subjected to steady shear is obtained as a function of S_c. Poiseuille flow in microchannels for fixed polymer concentration and varying number of repeated units within a chain is simulated. The nonuniform concentration profiles and their dependence on S_c are computed. We show the effect of the *bounce-forward* wall boundary condition on the depletion layer thickness. A power law fit of the velocity profile in stratified Poiseuille flow in a microchannel yields wall viscosities different from bulk values derived from uniform, steady plane Couette flow. The form of the velocity profiles indicates that the slip flow model is not useful for the conditions of these calculations. © *2006 American Institute of Physics*. [DOI: 10.1063/1.2360274]

I. INTRODUCTION

The essence of the dissipative particle dynamics (DPD) model is a particulate fluid with rare-gas number densities but with the compressibility of liquids. However, near incompressibility is insufficient to guarantee acceptable liquid behavior in dynamic problems. Groot and Warren[1] have identified diffusion as one of the deficiencies of the dynamics, and they demonstrated that self-diffusion Schmidt numbers (S_c) are effectively confined to the gaseous range of $\mathcal{O}(1)$. By means of kinetic theory for transport coefficients, it was shown in Ref. 2 and 3 that Schmidt numbers in the liquid range require prohibitively large values of number density ρ and/or cutoff radius r_c. Lowe[4] proposed an alternative scheme which replaces the explicit, thermally balanced, dissipative and random forces of the standard scheme with the Andersen thermostat.[5] This introduces the characteristic decay time for relative velocities Γ^{-1}, which controls the time step by $\Gamma\Delta t<1$, and is the principal parameter in Lowe's approximate formulas for the transport coefficients. In Ref. 6 extensions of single bead-spring chains immersed in shear fields were calculated by DPD and were shown to require solvent self-diffusion Schmidt numbers in the liquid range to be in agreement with the corresponding experimentally measured extensions of single λ-phage DNA molecules. Similar Brownian dynamics (BD) calculations show that agreement is close or not close depending on whether hydrodynamic interactions between beads is included[7] or is not included,[8] respectively. None of these simulations attempt to model the experimental solvent, an aqueous buffer solution whose viscosity is enhanced with dissolved sucrose. Thus, the agreement with experiment obtained by two rather different methods suggests that the Schmidt number effect is not an indicator of some complex diffusional mechanism but points to the importance of properly capturing hydrodynamic effects in DPD simulation. Peters[9] argues that self-diffusion coefficients of DPD particles cannot be equated with those of individual molecules and that this nullifies the arguments of Groot and Warren[1] and of Lowe[4] that require DPD to realize S_c of $\mathcal{O}(10^3)$, typical of liquids. What is shown in Ref. 6 and in this work is that agreement with experiment improves as S_c increases and that the effect saturates as liquid values are approached.

Classical analysis at the mesoscopic scale begins with the Langevin equation whose long-time solutions are the basis of Brownian dynamics. For a single free particle such solutions—with the inertia of both particle and solvent neglected—represent a balance between the drag force due to the continuous viscous solvent and the random Brownian force. Solvent DPD particles are point centers of repulsion which typically represent clusters of $\mathcal{O}(10^{10})$ molecules,[10] and if they are to statistically simulate a continuous viscous solvent they must satisfy certain conditions (equivalent to Brownian dynamics). Empirically, it has long been known[11] that coefficients of diffusion, D, and viscosity, μ, for spherical molecules yield Stokes-Einstein numbers in the range of $\frac{1}{4}\pi \geqslant D\mu a/k_BT \geqslant \frac{1}{6}\pi$, where the upper and lower bounds hold when the size a of the diffusing species, respectively, is the same as or is much larger than the solvent molecules. These bounds correspond to Einstein's original analysis with the hydrodynamic drag derived from boundary conditions of zero shearing traction (perfect slip) or of zero tangential velocity (no slip), respectively, and have been inferred[11] from

[a]Author to whom correspondence should be addressed. Electronic mail: sjoh0341@dam.brown.edu

experimental data on real systems. Brownian dynamics sheds no light on the transition from slip to no slip with the relative molecular, sizes since it assumes the solvent to be continuous. Here the bounds will be employed in the analysis of numerical experiments from which the transport coefficients are calculated, and by means of the Stokes-Einstein number a characteristic length a is then calculated. To be plausible as a length associated with a DPD particle, a should be less than the cutoff radius r_c. Pagonabarraga *et al.*[12] introduced a length $\lambda=\sqrt{2k_BT/m}/N_c\gamma/m$ where N_c is the average number of interacting particles of mass m and γ is the dissipative-force coefficient in the standard DPD scheme. Their results show that hydrodynamic response requires $\lambda<r_c$. The definition of the Stokes-Einstein length has the advantage of being independent of the parameters of any particular scheme.

The neglect of the solvent inertia in the motion of a diffusing particle immersed in a sheared solvent requires a small magnitude of the Reynolds number, $R_e=\dot{\gamma}a^2\rho_m/\mu$, where $\dot{\gamma}$ is the imposed shear rate and ρ_m is the mass density. In the case of self-diffusion, the diffusing-particle size is the same as the solvent's. Accordingly, the Stokes-Einstein number is equated to the upper bound given above, and then the Reynolds number can be expressed as $R_e=3\tau/(k_BT\rho S_c)=9v_*^2/(\bar{v}^2S_c)$. Here $\tau=\mu\dot{\gamma}$ and $v_*=\sqrt{\tau/\rho_m}$ are, respectively, the shear stress and the friction velocity of the macroscopic shear flow, $\bar{v}=\sqrt{3k_BT/m}$ is magnitude of the fluctuating velocity for a particle with mass $m=4\pi a^3\rho_m/3$, and $S_c=\mu/(\rho_m D)$ is the Schmidt number. Thus, the small Reynolds numbers required for DPD to be equivalent to Brownian dynamics can be maintained by controlling the product $k_BT\rho S_c$ for a given applied shear stress τ. Simultaneously, the third form of this Reynolds number shows that high Schmidt numbers are required as the friction velocity v_* increases relative to the fluctuating velocity $\bar{v}$.

The paper is organized as follows: Sec. II outlines the DPD method and the thermostats used; Sec. III defines the bead-spring models we employ; Sec. IV provides the transport coefficients for each scheme; Sec. V and VI show results for the response of wormlike chains under steady shear; Sec. VII gives results about S_c effects on polymers; and Sec. VIII and IX deal with depletion layer effects and boundary conditions. Lastly, Sec. X is a comparison between the apparent wall viscosity in Poiseuille flow and the one calculated from plane Couette flow. We conclude in Sec. XI with a brief summary and a discussion.

II. THE DPD EQUATIONS

We consider a system of N particles, each having mass m_i, whose momenta and position vectors are governed by Newton's equations of motion. In particular, for a typical particle i,

$$\mathbf{v}_i=\dot{\mathbf{r}}_i, \quad \mathbf{F}_i=m_i\dot{\mathbf{v}}_i, \tag{1}$$

where d/dt is denoted by overdot, $\mathbf{v}_i$ is the particle velocity, $\mathbf{r}_i$ is its position vector, and $\mathbf{F}_i$ is the net force. Throughout this work we choose $m_i=1$. The interparticle force $\mathbf{F}_{ij}$ exerted on particle i by particle j is composed of conservative ($\mathbf{F}_{ij}^c$), dissipative ($\mathbf{F}_{ij}^d$), and random ($\mathbf{F}_{ij}^r$) components. Hence the total force on particle i is given by

$$\mathbf{F}_i=\sum_{i\neq j}\mathbf{F}_{ij}^c+\mathbf{F}_{ij}^d+\mathbf{F}_{ij}^r. \tag{2}$$

The above sum acts over all particles within a cutoff radius r_c above which the forces are considered negligible. This interaction radius is set to $r_c=1$ and defines the length scale of the system. Denoting $\mathbf{r}_{ij}=\mathbf{r}_i-\mathbf{r}_j$, $\mathbf{v}_{ij}=\mathbf{v}_i-\mathbf{v}_j$, $\mathbf{r}_{ij}=|\mathbf{r}_{ij}|$, and the unit vector $\mathbf{e}_{ij}=\mathbf{r}_{ij}/r_{ij}$ we further define each of the forces to take the following forms:

$$\mathbf{F}_{ij}^c=F^{(c)}(r_{ij})\mathbf{e}_{ij}, \tag{3a}$$

$$\mathbf{F}_{ij}^d=-\gamma\omega^d(r_{ij})(\mathbf{v}_{ij}\cdot\mathbf{e}_{ij})\mathbf{e}_{ij}, \tag{3b}$$

$$\mathbf{F}_{ij}=\sigma\omega^r(r_{ij})\xi_{ij}\mathbf{e}_{ij}, \tag{3c}$$

where ξ_{ij} are symmetric Gaussian random variables with zero mean and unit variance and σ and γ are *not* independent, as shown below. Newton's equations of motions govern each particle's motion through

$$d\mathbf{r}_i=\mathbf{v}_i\delta t, \tag{4a}$$

$$d\mathbf{v}_i=\frac{\mathbf{F}_i^c\delta t+\mathbf{F}_i^d\delta t+\mathbf{F}_i^r\sqrt{\delta t}}{m_i}, \tag{4b}$$

where the factor $\sqrt{\delta t}$ appears because the random forces are interpreted as Wiener processes.

The conservative force $\mathbf{F}_{ij}^c$ is similar to that in the molecular dynamics (MD) formulation. It can be any force derivable from a predefined potential and can be tailored to each individual simulation problem. Possible choices include electrostatic forces, linear and nonlinear springs, van der Waals, hard repulsions (Lennard-Jones), or soft repulsions (potential preaveraged forces in the spirit of Ref. 13). Hence, $\mathbf{F}_{ij}^c$ is not constrained or defined by the DPD equations. This force as well as the other two act within a sphere of radius r_c, which defines the length scale of the system; it corresponds to a *soft repulsive-only* interaction potential. By averaging the Lennard-Jones potentials or the corresponding molecular field over the *rapidly* fluctuating motions of atoms over short time intervals, an effective average potential is obtained. A linear approximation of this is as follows:[1]

$$F^{(c)}(r_{ij})=\begin{cases}a_{ij}(1-r_{ij}/r_c) & \text{if } r_{ij}\leqslant r_c\\ 0 & \text{if } r_{ij}>r_c.\end{cases} \tag{5}$$

Unlike the hard Lennard-Jones potential which is unbounded at $r=0$, the *soft potential* employed in DPD has a finite value a_{ij} at $r=0$. The dissipative and random forces, on the other hand, are characterized by strengths $\omega^d(r_{ij})$ and $\omega^r(r_{ij})$ coupled by the *fluctuation-dissipation* relations,[14]

$$\omega^d(r_{ij})=[\omega^r(r_{ij})]^2=\begin{cases}(1-r_{ij}/r_c)^2 & \text{if } r_{ij}\leqslant r_c\\ 0 & \text{if } r_{ij}>r_c,\end{cases} \tag{6a}$$

$$\sigma^2=2\gamma k_BT. \tag{6b}$$

The fluid simulated by the DPD method is strongly dependent on the thermostat used, which in effect defines the time-

marching integrator of the underlying equations. The two basic DPD integrating schemes we will consider in this work are a modified version of the classical velocity-Verlet algorithm (vV)—as outlined by Groot and Warren[1]—and Lowe's algorithm.[4,15]

The vV scheme is characterized by explicit calculation of all forces $\mathbf{F}^c$, $\mathbf{F}^d$, and $\mathbf{F}^r$ (conservative, dissipative, and random) and is known to be time step dependent, but at the same time straightforward and relatively accurate. The vV DPD scheme relies on a basic predictor-corrector approach, which uses provisional values of the velocities for the force calculations, which are corrected at the end of each time step. It is important to keep in mind that the DPD dissipative forces depend on the relative velocities of the particles, hence this prediction is crucial.

Lowe's method[4] employs the Andersen thermostat[5] with the particle velocities corrected at every timestep using the Maxwell velocity distribution. In the absence of conservative forces, which are integrated in the vV manner, the scheme is shown to be independent of the time step Δt,[15] although a recent work[16] has shown that the scheme can give rise to some minor artifacts. The core operation in Lowe's method involves the reequilibration of the particle momenta at one step with an updated interparticle relative velocity drawn from a Gaussian distribution. The scheme is characterized by the explicit calculation of $\mathbf{F}^c$ and the subsequent reequilibration of all particle velocities. This is done using the *relative* velocities of particle pairs. The method conserves momentum and introduces an extra parameter Γ so that, in the limiting case of $\Gamma\Delta t \approx 1$, thermalization/dissipation occurs at every time step for all neighbors of the particular DPD particle examined. Peters[9] recently introduced a modification of Lowe's scheme by keeping the centroid velocity of a particle pair unchanged before and after the reequilibration. This results in an attractive scheme, still independent of the chosen time step (as opposed to the Verlet approach) that also discretizes the original DPD equations (Lowe's method does *not*). An overview of the original Lowe scheme is given in Ref. 15.

We stress that the fundamental difference between Lowe's and the vV scheme is that dissipative and random forces are not explictly calculated in the former.

III. THE FENE AND WORMLIKE CHAINS

In our simulations bead-spring representations of polymeric chains move freely in a DPD solvent of N particles. These chains consist of beads (DPD particles) subject to the standard DPD forces: soft repulsive (conservative), dissipative, and random. *In addition* to these forces, they are subject to intrapolymer forces, arising from different combinations of spring laws between consecutive beads on a chain (bonded interactions). Excluded volume repulsions (nonbonded interactions) are not considered in this work. The two spring laws used in this work are defined below.

- FENE spring. Within a chain of M beads each bead is subject to a pairwise nonlinear spring force. The finitely extensible nonlinear elastic (FENE) spring has a maximum extensibility $r_{\max}$ beyond which the force becomes infinite, and hence any length greater than $r_{\max}$ is considered unphysical and is not allowed. The potential is described by

$$U_{\mathrm{FENE}} = -\frac{\kappa}{2} r_{\max}^2 \log\left[1 - \frac{|\vec{r}_i - \vec{r}_{i-1}|^2}{r_{\max}^2}\right],$$

$$\text{where } i = 2,3,4,\ldots,M$$

and κ is the spring constant. The interbead force is $\mathbf{F}^c = -\nabla U_{\mathrm{FENE}}$.

- Marko-Siggia wormlike chain. Polymers of biological importance (DNA and proteins) are thought to be structurally stiff. The wormlike chain model[17–19] can be thought of as a continuous curve in three-dimensional space. Its *persistence length* λ_p measures the chain's stiffness and is the average length over which the orientation of a curved segment is unchanged ("persists"). We will focus on the bead-spring representation of the model, which approximates a portion of the wormlike chain with a force law given by the Marko-Siggia[20] expression,

$$F^{(c)} = \frac{k_B T}{\lambda_p}\left[\frac{1}{4(1-R)^2} - \frac{1}{4} + R\right],$$

where

$$R = \frac{|\vec{r}_i - \vec{r}_{i-1}|}{L_{\mathrm{spring}}} = \frac{r}{L_{\mathrm{spring}}}, \quad i = 2,3,4,\ldots,M$$

and L_{spring} is the maximum allowed length for each chain (spring) segment. The expression is accurate for large values of the ratio $L_{\mathrm{spring}}/\lambda_p$ and exact as $r \to 0$ or $r \to L_{\mathrm{spring}}$.

The Marko-Siggia spring law is an averaged quantity, locally approximating flexible rods. The derivation of the formula accounts for coarse-graining microscopic elements of a long chain (such as bead rod) by use of statistical mechanics. However, in order to use the Marko-Siggia law in molecules with more than two beads (dumbbells), some authors[21] account for the different stiffnesses of the beaded counterparts by altering the persistence length λ_p of the subchains. Detailed analysis of such arguments[22] has shown that it is possible to minimize the errors arising by the introduction of beads and subchains. Throughout this work we will adopt the analysis presented in Ref. 22 for stained λ-phage DNA molecules assumed to have $L = 21.1\ \mu$m (fully extended length) and $\lambda_p = 0.053\ \mu$m (persistence length). The correction we will apply will linearly approximate the ratio of effective to true persistence length for three different regions of the extension: low-force, half-extended spring, and high-force regimes. More specifically, we define the ratio

$$\lambda^\star = \frac{\lambda_p[\text{effective}]}{\lambda_p[\text{true}]},$$

so that when $\lambda^* = 1$ no correction is applied. The tables in Ref. 22 suggest high, medium, and zero corrections for the low-force, half-extension, and high-force regions, respectively. We go one step further to introduce a linear fit to the

suggested correction values for N-bead chains,

$$\lambda^{\star} \approx (1.0 - \hat{z})0.022(N-1) + 1 \quad \text{if } N \leqslant 20,$$

$$\lambda^{\star} \approx (1.0 - \hat{z})0.025(N-1) + 1 \quad \text{if } N > 20,$$

where $0 \leqslant \hat{z} \leqslant 1$ is the instantaneous fractional extension of the whole molecule in the stretching direction. The above expressions approximate fairly accurately the values given in Ref. 22 and are implemented in all instances of $N > 2$ for the Marko-Siggia spring force in this work.

IV. DYNAMICS: THE SCHMIDT NUMBER

The characterization of the simulated fluid in DPD is of major importance for the understanding of the strengths and weaknesses of the method. In this section we examine fundamental quantities, such as kinematic viscosity $\nu = \mu/\rho$ and diffusion coefficient D and their dependence on the specific parameters of each DPD integrating scheme.

The peculiar velocity $\tilde{\mathbf{u}}_i$ of particle i is defined as $\tilde{\mathbf{u}}_i = \mathbf{u}_i - \bar{\mathbf{u}}(\mathbf{x})$, where $\bar{\mathbf{u}}(\mathbf{x})$ is the stream velocity at position $\mathbf{x}$. For a system of N particles of mass m_i each the $\alpha\beta$ component of the stress tensor is given by the Irving-Kirkwood formula,[23]

$$S_{\alpha\beta} = -\frac{1}{L_x L_y L_z}\left\langle \sum_{i=1}^{N} m_i \tilde{u}_{i\alpha}\tilde{u}_{i\beta} + \sum_{i=1}^{N}\sum_{j>i}^{N} r_{ij\alpha}F_{ij\beta} \right\rangle, \tag{7}$$

where $F_{ij\beta}$ is the β component of the net force acting on particle i due to particle j and $r_{ij\alpha}$ is the α component of their relative position vector. It is interesting to note here that Eq. (7) is directly applicable in its current form to the velocity-Verlet method but *not* to Lowe's scheme, which lacks explicit calculation of dissipative/random forces. To this end, we propose a modification of Eq. (7) to incorporate the velocity reequilibrations $\mathbf{\Delta}_{ij}$ in Lowe's scheme interpreted as an additional force term,

$$S_{\alpha\beta} = -\frac{1}{L_x L_y L_z}\left\langle \sum_{i=1}^{N} m_i \tilde{u}_{i\alpha}\tilde{u}_{i\beta} + \sum_{i=1}^{N}\sum_{j>i}^{N} r_{ij\alpha}F_{ij\beta} + \sum_{i=1}^{N}\sum_{j>i}^{N} m_i r_{ij\alpha}\frac{\Delta_{ij\beta}}{\Delta t} \right\rangle, \tag{8}$$

where Δt is the simulation time step. The dynamic viscosity μ is determined with the fluid undergoing uniform shear at a rate $\dot{\gamma}$ through the total shear stress S_{xy} (x is the direction of the shear and y is the wall-normal direction) by

$$\mu = \frac{S_{xy}}{\dot{\gamma}}, \quad \dot{\gamma} = \frac{U_x}{L_y},$$

and therefore the kinematic viscosity is $\nu = \mu/\rho = \mu L_x L_y L_z/N$. (The shear rate $\dot{\gamma}$ is not to be confused with the dissipative-force coefficient γ.)

The viscosity was also computed through the *periodic Poiseuille flow* method, suggested by Backer *et al.*[24] The method consists of simply superimposing a constant force g_x or $-g_x$ in the x direction for all particles i with $\mathbf{r}_{i_y} > L_y/2$ or $\mathbf{r}_{i_y} < L_y/2$, respectively. Then, for a periodic simulation box of length L_y in the y direction, number density ρ, velocity profile $U(y)$ in the x direction, and dynamic viscosity μ, we find that

$$\frac{\rho g_x (L_y/2)^2}{12\mu} = \frac{2}{L_y}\int_{y=0}^{y=L_y/2} U(y)dy.$$

Viscosities calculated by these two methods gave agreement to within 1 part in 10 000.

The self-diffusion coefficient D is computed by use of the velocity autocorrelation function (VAF), $C_u|_{t=T} = (1/N)\Sigma_{i=1}^{N} \mathbf{u}|_{t=0} \cdot \mathbf{u}|_{t=T}$, through the Green-Kubo integral $1/3\int_{t=0}^{t=\infty} C_u(t)dt$.

The fundamental differences between the vV and Lowe's scheme manifest themselves in the values of the self-diffusion coefficient D, the viscosity ν, and eventually the Schmidt number $S_c = \nu/D$ characterizing the simulated fluid. Groot and Warren[1] showed that the vV method for a number density $\rho = 3$ and a dissipation amplitude $\gamma = 6.75$ produced Schmidt number values close to those predicted by the theory but too small (by three orders of magnitude) to simulate real liquids. We investigate this issue next.

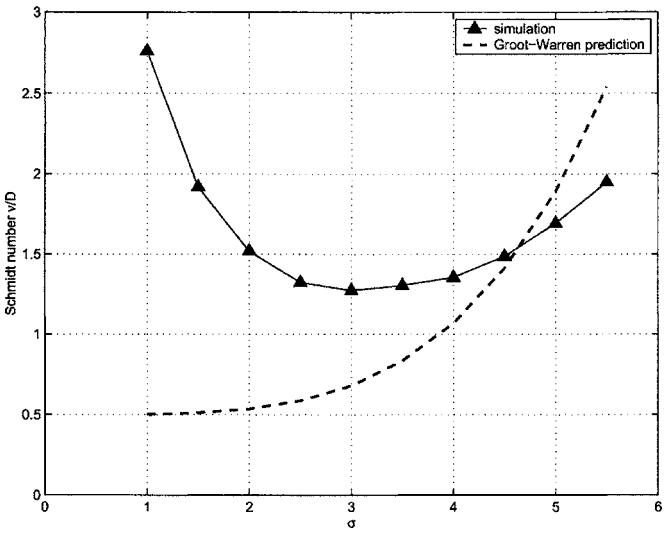

FIG. 1. Schmidt number S_c plotted against σ for vV. The Schmidt number is $\mathcal{O}(1)$. Here $k_B T = 1$.

A. The Schmidt number for the velocity-Verlet scheme ($\delta t = 0.01$)

In order to investigate the effect of the dissipative- and random-force coefficients γ and σ on the fluid, we compute S_c for a wide range of values. Figure 1 shows the computed Schmidt numbers for a 4000-particle fluid, in a $10 \times 10 \times 10$ sized box with a time step $\delta t = 0.01$ and a conservative force coefficient $a_{ij} = 75 k_B T/\rho$. In the figure we also compare our computed results with a theoretical estimate presented in Ref. 1 for ideal gas conditions, namely,

$$S_c \approx \frac{1}{2} + \frac{(2\pi\gamma\rho r_c^4)^2}{70875 k_B T}. \tag{9}$$

For the viscosity calculations we apply a constant force of magnitude $g_x = 1$ as previously described to obtain a periodic Poiseuille profile. Groot and Warren[1] correctly argued that the vV scheme produces unrealistic values for S_c. The calcu-

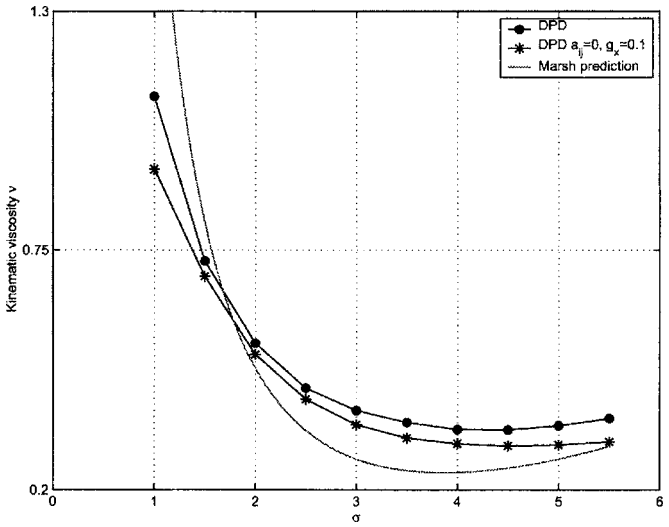

FIG. 2. Kinematic viscosity ν plotted against σ for ideal gas and water repulsion parameters; the solid line corresponds to the theoretical ideal gas expression (Ref. 3).

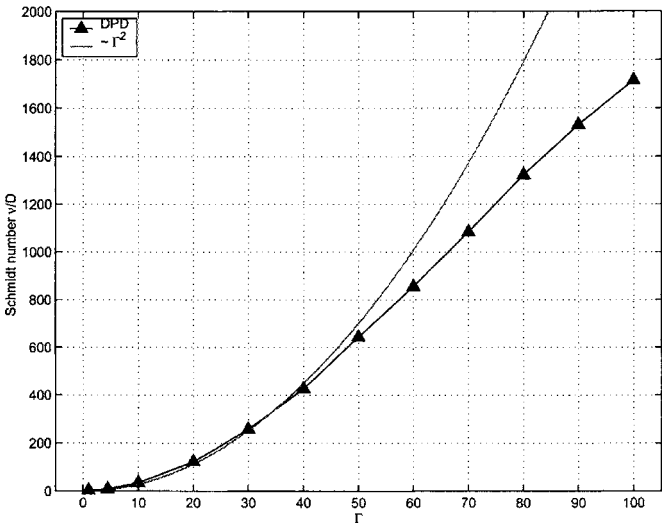

FIG. 3. Schmidt number S_c plotted against Γ for Lowe's scheme with $\delta t=0.01$. The Schmidt number is $\mathcal{O}(10^3)$. Here $k_BT=1$.

lated value of $S_c=1.00\pm0.03$ for $\sigma=3.67$ and $\rho=3$ provided in Ref. 1 is in reasonable agreement with the one shown here ($S_c\sim1.3$ for $\sigma=3.5$ and $\rho=4$). The main point here is that the Schmidt number is $\mathcal{O}(1)$ for the vV method. Marsh's[2,3,24] theoretical estimate on the kinematic viscosity $\nu(\sigma)$ for an ideal gas consists of a dissipative term that transfers momentum through particle collisions ($\sim\sigma^2$) and a kinetic contribution that transfers momentum through particle motion and displacement ($\sim\sigma^{-2}$), namely,

$$\nu(\sigma)=\frac{45(k_BT)^2}{2\pi\sigma^2r_c^3\rho}+\frac{\pi\rho\sigma^2r_c^5}{1575k_BT}. \tag{10}$$

Figure 2 shows a reasonable agreement of the ideal gas prediction with the computed results. We compare the analytical expression (10) with the DPD values for conditions corresponding to ideal gas ($a_{ij}=0$) and water ($a_{ij}=75k_BT/\rho$). Next, we examine similar quantities for Lowe's scheme.

B. The Schmidt number for Lowe's scheme ($\delta t=0.001,0.01$)

In order to investigate the effect of Lowe's thermalization parameter Γ on the fluid, we compute S_c for a wide range of values. Figure 3 shows the computed Schmidt numbers for a 4000-particle fluid, under the conditions described above.

We investigate the described system for Lowe's scheme and its dependence on the parameter Γ. To this end, we perform one series of simulations with $\delta t=0.001$ and one with $\delta t=0.01$. However, Γ is varied so that $\Gamma\delta t\in[1,1000]\times0.001=[0.001,1]$ and $\Gamma\delta t\in[1,100]\times0.01=[0.01,1]$, respectively.

For an ideal dissipative gas, Lowe's thermostat is governed by two distinct time scales, as shown in Ref. 4; a typical time t_1 it takes a particle to travel a distance r_c with a given velocity and a typical time t_2 it takes the velocity correlations to decay. Assuming the latter to be dependent only on Γ, we have

$$t_1=\sqrt{\frac{mr_c^2}{k_BT}},\quad t_2=\frac{1}{\Gamma}\Rightarrow\Lambda=\frac{t_2}{t_1}=\sqrt{\frac{k_BT}{mr_c^2\Gamma^2}}.$$

Hence, under the assumption that the velocity correlations decay in time is $\tau_D\sim1/\Gamma$, Lowe's scaling for the kinematic viscosity $\nu=\pi\rho\Gamma r_c^5/75m$ can be used to show the Schmidt number,

$$S_c=\frac{\text{viscosity}}{\text{diffusivity}}=\frac{\nu}{D}=\frac{\pi\rho\Gamma r_c^5/75m}{k_BT\tau_D/m}\sim\frac{1}{\Lambda^2}\sim\frac{\Gamma^2}{k_BT}. \tag{11}$$

Lowe, in his original paper,[4] derived the above scaling, and our results in both Figs. 3 and 4 verify this trend to be true for Γ values satisfying $0\leqslant\Gamma\delta t\leqslant0.5$. We anticipate the disagreement for large Γ values to improve if indeed a dissipative gas ($a_{ij}=0$) is simulated; in our simulations $a_{ij}=75k_BT/\rho$. Lowe's method shows great potential in addressing the issue of realistic S_c values, since for the examined range of parameters the maximum S_c reaches values of

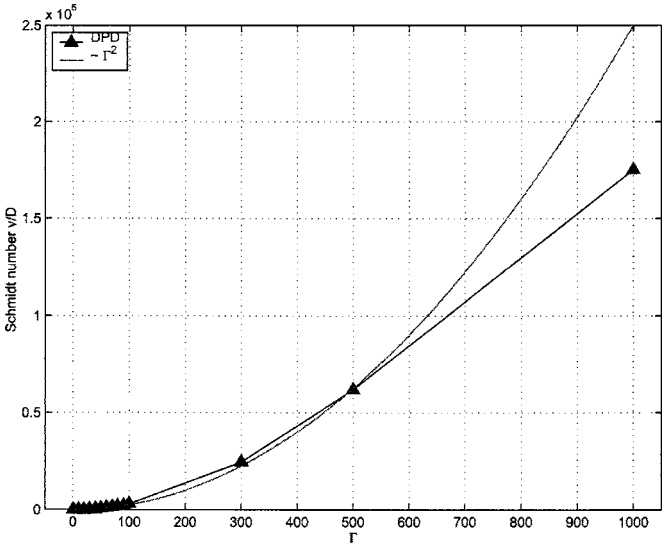

FIG. 4. Schmidt number S_c plotted against Γ for Lowe's scheme with $\delta t=0.001$. The Schmidt number is $\mathcal{O}(10^5)$. Here $k_BT=1$.

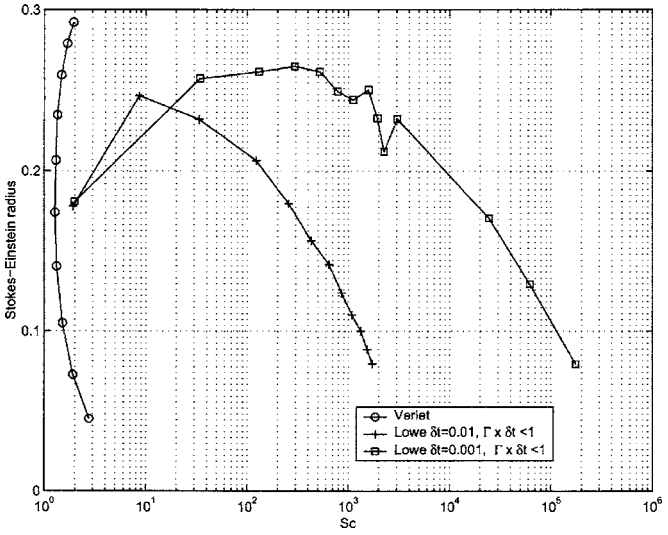

FIG. 5. The Stokes-Einstein radius a/r_c for the vV and Lowe's schemes plotted against $\log(S_c)$.

$\mathcal{O}(10^5)$, i.e., five orders of magnitude larger than those of velocity Verlet, for the same computational CPU requirements. Figures 3 and 4 show the dependence of the computed D, ν, and S_c on Γ.

Here we note that the diffusion coefficient scales as $1/\Gamma$ and it is approximately independent of the size of the time step despite the fact that the product $\Gamma\Delta t$ controls the thermalization process in Lowe's method. Indeed, we found that the relaxation time for a five-bead worklike chain (WLC) scales roughly as $\sim\Gamma$ for Lowe's method. Intuition supports this, since viscosity scales linearly with Γ as well.

With D and ν in hand, the Stokes-Einstein radius is computed from the Stokes-Einstein formula $a=1/4\pi k_B T D\mu$ and the result is shown in Fig. 5 as a function of S_c. Once again, the vV scheme is limited to low S_c and appears to give anomalous behavior because the scheme does not yield valid diffusivities. In all three cases, the value of a is approximately $r_c/5$. For $\rho=4$ the average number of interacting particles is about 17, and it is easily verified that if each particle has radius a these particles will easily fit into a sphere r_c.

V. SHEAR RESPONSE OF WORMLIKE CHAINS

The results presented in this section aim to simulate the response of λ-phage DNA molecules under steady shear and compare the DPD results with corresponding results from Brownian Dynamics (BD)[8] and experimental[25] data. The WLC described in Sec. III is used for all DNA simulations, and Underhill and Doyle's[22] persistence length (λ_p) correction always applies to our results for $M>2$. The correction of Bouchiat *et al.*[26] for the dumbbell case produced statistically similar results to the original Marko-Siggia (MS) model. Since the λ_p correction studies in Ref. 22 were done with the MS formula, we do not use the version of Bouchiat *et al.*.

DNA molecules under steady shear have been extensively studied in experimental[25] and computational[7,8] works. In 1999, Smith *et al.*[25] performed a benchmark study of λ-DNA molecules in uniform shear flow of shear rates $\dot\gamma < 4.0(1/\mathrm{s})$ employing a ~ 50 μm gap in solvents with viscosities $\mu=60$ and 220 cP. These stained bacteriophage molecules have a contour length $L\sim 21$ μm and longest relaxation times of 6.3 s (in the 60 cP solution) and 19 s (in the 220 cP solution). A typical molecule contains roughly 400 persistence lengths and hence can be considered *flexible*. Using DPD we investigated the dynamics of a single WLC. The moving boundaries at $y=0$ and $y=L_y$ are modeled using the Less-Edwards boundary conditions:[27] particles leaving the domain at $y=0$ and L_y are advanced/retarded by increments of $\Delta r=U_x t$ and $-U_x t$, respectively, in the x direction, where t is the time elapsed from an appropriate origin of times and U_x denotes twice the shear velocity of each boundary. Moreover, the velocity of the particle is increased/decreased by U_x or $-U_x$, accounting for both the imposed boundary condition and the velocity discontinuity between the two walls. This correction is essential, since the dissipative forces depend on the relative pairwise velocities. The rest of the boundaries are treated periodically for all the solvent DPD particles. To avoid unphysical periodicity artifacts, polymer beads *only* undergo an elastic collision in the y direction: $(u,v,w)_{\mathrm{bead}} \rightarrow (u,-v,w)_{\mathrm{bead}}$ and $r_y \rightarrow r_y-(\Delta t)v_{\mathrm{bead}}$. Different chain sizes were accommodated by storing the polymer coordinates without mapping them back in the original domain. This allowed the intrapolymer forces to be calculated properly, while the collective solvent-solvent and polymer-solvent interactions were calculated with the mapped (periodic) images. The effect of the simulation box size $L_x\times L_y\times L_z$ for the presented results was investigated and proved to be negligible. For the results shown, a periodic box of dimensions $10\times 20\times 5$ was used in a fluid of 4000 DPD particles. The conservative force amplitude was fixed to $a_{ij}=75k_BT/\rho$, as in Ref. 1.

In order to properly simulate λ-phage DNA molecules under steady shear, we define the dimensionless Weissenberg number of the flow as $W_e=\dot\gamma\tau$, for a shear rate $\dot\gamma$. Here, τ is the polymer's longest relaxation time, which is computed by fitting an exponential analytical curve to the average mean-square extension; this is *not* necessarily the end-to-end value. This approach provides a relaxation time nearly the same (within 10%) with that obtained by fitting the late-time tail of the mean-square radius of gyration $\langle R_g^2\rangle$. The calculated mean-square extension of an initially 30%-extended chain was fitted with $\langle x^2\rangle=\langle x^2\rangle_0+x_i^2 e^{-t/\tau}$ to obtain the chain relaxation time τ. Here, x_i^2 is the initial stretch and $\langle x^2\rangle_0$ is the equilibrium value. Equating the area under both curves fixed the free parameter of the fit.

VI. WORMLIKE CHAIN AND LOWE'S SCHEME: $S_c\approx 35$, 690, AND 2574

The Schmidt number results presented in Fig. 3 motivate the comparison of the mean fractional extension of a wormlike chain molecule under shear. Figure 6 shows the calculated average molecular (maximum projected) extension versus W_e. The DPD results are compared with BD (Ref. 8) and experimental DNA data[25] for three different S_c, using Lowe's scheme. We focus on a five-bead WLC and three different cases: $S_c\approx 35(\Gamma=4.5)$, $S_c\approx 690(\Gamma=22)$, and $S_c\approx 2574(\Gamma$

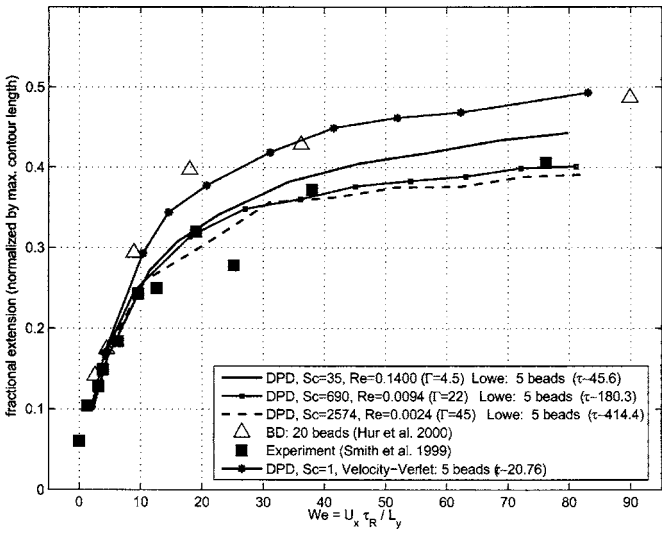

FIG. 6. Time-averaged mean fractional extension of a five-beaded wormlike chain under shear vs W_e for $\Gamma=4.5$ ($S_c\approx 35$), $\Gamma=22$ ($S_c\approx 690$), and $\Gamma=45$ ($S_c\approx 2574$). Here $k_BT=0.2$. An empirical approximate formula would be $S_c\approx 1.4\Gamma^2$, in agreement with Lowe's arguments (Ref. 4). For reference we provide the data for the vV scheme ($S_c\sim 1$).

$=45$). The temperature was kept constant at $k_BT=0.2$. Figure 6 shows an agreement of the averaged values with the experimental data for the higher S_c, verifying the consistency of the viscosity and diffusion calculations that the powerful alternative Lowe's scheme provides through the adjustment of Γ. Moreover, of interest is the monotonic dependence of the curves on S_c. For reference we provide the data for the vV scheme ($S_c\sim 1$). The uncertainties of the extension curves, measured through the standard deviation, vary with W_e. A typical error bar value for low W_e is 4% of the fractional extension, while for $W_e\approx 80$ is 11%. The Reynolds number R_e defined in the introduction, is also given in Fig. 6 for the highest shear rates corresponding to $W_e\approx 80$. This Reynolds number varies as $\sim 1/S_c$ as expected and attains small values as S_c approaches the liquid range. For $S_c\sim\mathcal{O}(1)$, R_e is about 5, well beyond the Stokes flow range. The overprediction of the extension in BD simulations was also observed by other research efforts[28] where DPD was also used to characterize the solvent (poor, near θ, and good).

The self-consistency of the parameters was verified from the equilibrium mean-square end-to-end distance of a two-bead dumbbell, computed as $\langle S^2\rangle\approx 8.56$, in close agreement with the theoretical value of 8.92 given by[19] $\langle S^2\rangle=2L_{\rm sp}\lambda_p(1-(\lambda_p/L_{\rm sp})(1-e^{-L_{\rm sp}/\lambda_p}))$.

VII. EFFECT OF SCHMIDT NUMBER ON POLYMERIC QUANTITIES

In this section we investigate the effect of S_c on the size of polymeric chains (measured through the mean square radius of gyration $\langle R_g^2\rangle=\langle(1/M\Sigma_{i=1}^{M}(R_i-R_{\rm cm})^2\rangle$) in equilibrium and steady shear, as well as their longest relaxation time τ. To this end, we refer to Eq. (11) to verify $S_c\sim\Gamma^2/k_BT$. Table I summarizes ν, D, and S_c values for different combinations of Γ and k_BT. We include column IV as baseline vV case for comparison. We use polymeric chains subject to FENE springs, with maximum extensibility $r_{\rm max}=5r_c$, spring constant $\kappa=30k_BT$, and number of beads per chain $M=5$. The relaxation time for cases $S_c=\mathcal{O}(1)$ (columns IV and V) are crude approximations, since the corresponding relaxation curves do not follow exponential ones at such low values of S_c. Several conclusions can be drawn from the entries of Table I.

TABLE I. Dependence of different static and dynamic quantities on Lowe's parameter, Γ, vV parameter σ, and temperature k_BT ($\kappa=30k_BT$, $r_{\rm max}=5r_c$).

Column	I	II	III	IV	V
	Lowe $\Gamma=1$, $k_BT=0.01$	Lowe $\Gamma=10$, $k_BT=1$	Lowe $\Gamma=50$, $k_BT=1$	vV $\sigma=3$, $k_BT=1$	Lowe $\Gamma=0.45$, $k_BT=1$
ν	0.1700	1.7240	9.5370	0.2784	0.2866
D	0.0046	0.0497	0.0149	0.2915	0.3100
Sc	~37	~35	~642	~0.96	~0.93
FENE: $\langle R_g^2\rangle$	0.2244	0.2245	0.2250	0.2241	0.2241
FENE: τ	11.1	0.770	4.75	~0.262	~0.318
FENE: $\langle R_g^2\rangle$ under shear with $\dot\gamma=\frac{1}{2}$	0.9486	0.2488	0.3809	0.2264	0.2270
$W_e=\dot\gamma\tau$	5.550	0.385	2.375	0.131	0.159

- Columns I and II verify Lowe's prediction of Eq. (11), since the Schmidt numbers agree. More specifically, $S_c\sim\Gamma^2/k_BT=1^2/0.01=10^2/1$.
- Columns IV and V correspond to two distinct cases (vV and Lowe) having $S_c\sim 1$. It is, therefore, possible to tune Lowe's parameter Γ so that the vV fluid is properly simulated. Values of both static and dynamic properties (ν, D, S_c, τ, and $\langle R_g^2\rangle$) show reasonable agreement.
- The near equality of all $\langle R_g^2\rangle$ values suggests that the effect of S_c on a FENE chain in equilibrium is minimal. In other words, a flexible chain in a solvent of DPD particles assumes more or less the same average size in equilibrium, regardless of the fluid surrounding it.
- Columns I and II suggest that solvent Schmidt number alone does not determine the longest relaxation time τ.
- Columns II–V suggest that the size of the chain under steady shear is directly affected by the Schmidt number of the solvent at constant temperature; the disagreement between columns I and II for the shear $\langle R_g^2\rangle$ values might be due to the difference in the root-mean-square velocity of the solvent particles ($\sqrt{\bar{v}^2}=\sqrt{3k_BT/m}$) and the shear velocity (constant for all columns), since the former is a function of k_BT. Indeed, the root-mean-square values of the velocity components are $|\bar{v}|\approx 0.08$ for $k_BT=0.01$ and $|\bar{v}|\approx 0.8$ for $k_BT=1$.

VIII. POLYMER CONCENTRATION IN POISEUILLE FLOW

Using the parameters presented in Table I, we aim to demonstrate that Lowe's method of $\Gamma=0.45$ can efficiently

TABLE II. Driving force for different Schmidt number fluids, as directed by the Newtonian fluid viscosity ratios, in order to recover similar Poiseuille profiles.

Fluid at $k_BT=1$	Lowe $\Gamma=10$	Lowe $\Gamma=50$	vV $\sigma=3$	Lowe $\Gamma=0.45$
Sc	~35	~642	~0.96	~0.93
g_x	0.02×6.1925	0.02×34.2565	0.02	0.02×1.0295

simulate the Verlet fluid of $\sigma=3$, as well as present Schmidt number effects on the polymer concentration depletion layer close to the wall. To this end we employ FENE springs with $\kappa=6k_BT$ and $r_{\max}=2r_c$ in a dilute solution of polymer concentration $\phi=$bead particles/total particles$=0.1087$. The total (solvent and bead) number of particles is $N=16\,000$, the number density $\rho=4$, and the domain is a periodic cube of side length $15.874r_c$.

The Poiseuille profile is sustained by the method described in Sec. IV, based on the setup of Ref. 24, and therefore the lower half of the domain is a "mirrored" periodic image of the upper half. The body force g_x is adjusted in each case so that it reflects the necessary pressure gradient according to the Newtonian viscosity ratios, with the corresponding values shown in Table II.

We examine polymer distribution effects for constant concentration $\phi=0.1087$ but varying beads per polymer chain, namely, 5-, 10-, and 60-bead FENE chains. In all presented results, the Weissenberg number $W_e=\dot{\gamma}\tau$ for given beads per chain is constant and directed by the driving force of the Newtonian cases. The Schmidt number, however, is the varying quantity. The fluid solvents we attempt to simulate are the ones found in Table II: a velocity-Verlet fluid ($\sigma=3$), Lowe's fluid with the same Schmidt number ($\Gamma=0.45$), and two Lowe fluids of higher Schmidt numbers.

Figures 7–9 show the dependence of center-of-mass (left) and bead (right) concentration on S_c plotted against the distance from the domain's "walls" (the use of nonperiodic wall boundary conditions is examined in Sec. IX). The depletion layer in all cases is strongly dependent on S_c and decreases with increasing S_c. Interestingly, as the beads per polymer chain increase, the dependence is more pronounced, with the 60-bead center-of-mass depletion layer reduced by half from $S_c\sim1$ to ~642 (Fig. 9, left). Such effect is not observed in the lower case of five-beaded chains, where the effect is minimal. Another notable point is the fact that indeed the two fluids of the last two columns of Table II give rise, in most cases, to similar distribution profiles, indicating indeed that the velocity-Verlet fluid *can* be simulated by an appropriate Lowe fluid.

The fully developed velocity profiles $U_x(y)$ for the two lower S_c number fluids are shown in Fig. 10. In the figures, the time- and bin-averaged velocity data are represented by solid squares, while a power law profile, governed by

$$U_x(y)=U_{\max}\left[1-\left(\frac{|y|}{0.5L_y}\right)^{1/n+1}\right],$$

has been fitted in each case, represented by solid lines. The dotted line represents the Newtonian, $n=1$ Poiseuille profile. Both figures reconfirm the similarity of the Verlet and Lowe low S_c fluids, with a power law close to $n=0.7$. Similar studies (not shown here) for the high S_c Lowe fluids show a less pronounced ($n\sim0.8$) power law fit.

IX. EFFECT OF BOUNDARY CONDITIONS IN PERIODIC POISEUILLE FLOW

The results presented so far employed the dual-Poiseuille profile described in Sec. IV. Elastic collisions confine the beads belonging to polymer chains in the domain along the y direction, but *no* similar confinement for the solvent DPD particles was enforced. These particles were free to migrate through periodic boundaries, without wall boundary conditions. Solid walls were not accounted for in the resulting polymer concentration distributions. In this section we demonstrate the effect of such boundary conditions

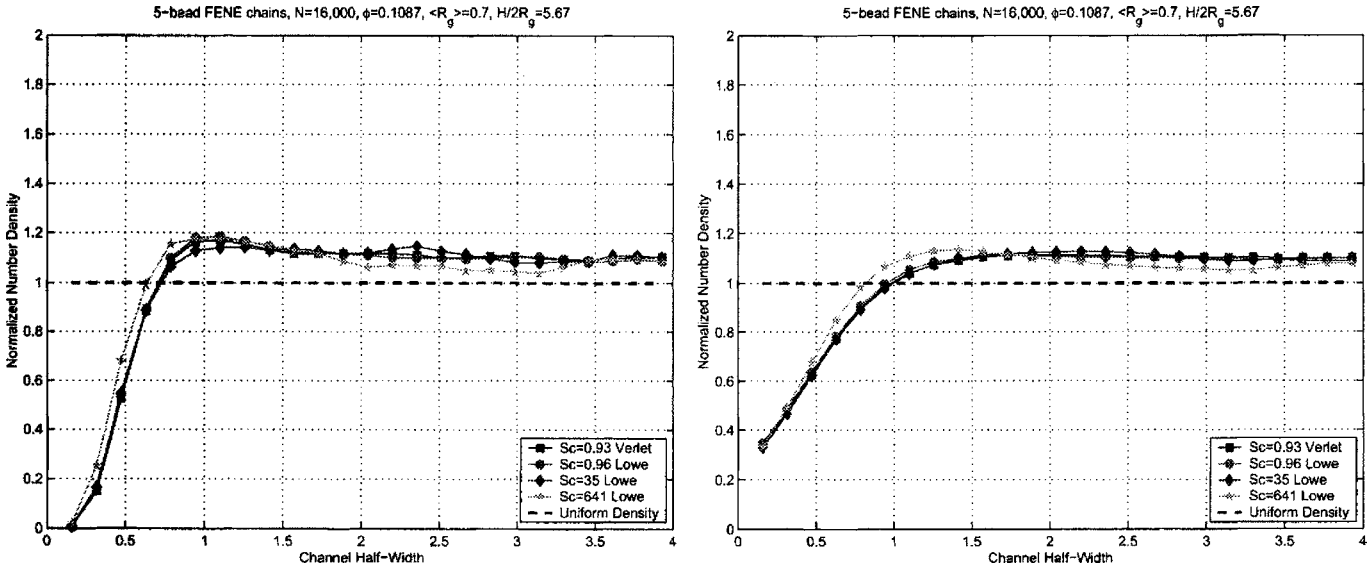

FIG. 7. Normalized polymer number density for five-bead chains as a function of the distance from the wall for the chain center of mass (left) and beads belonging to chains (right).

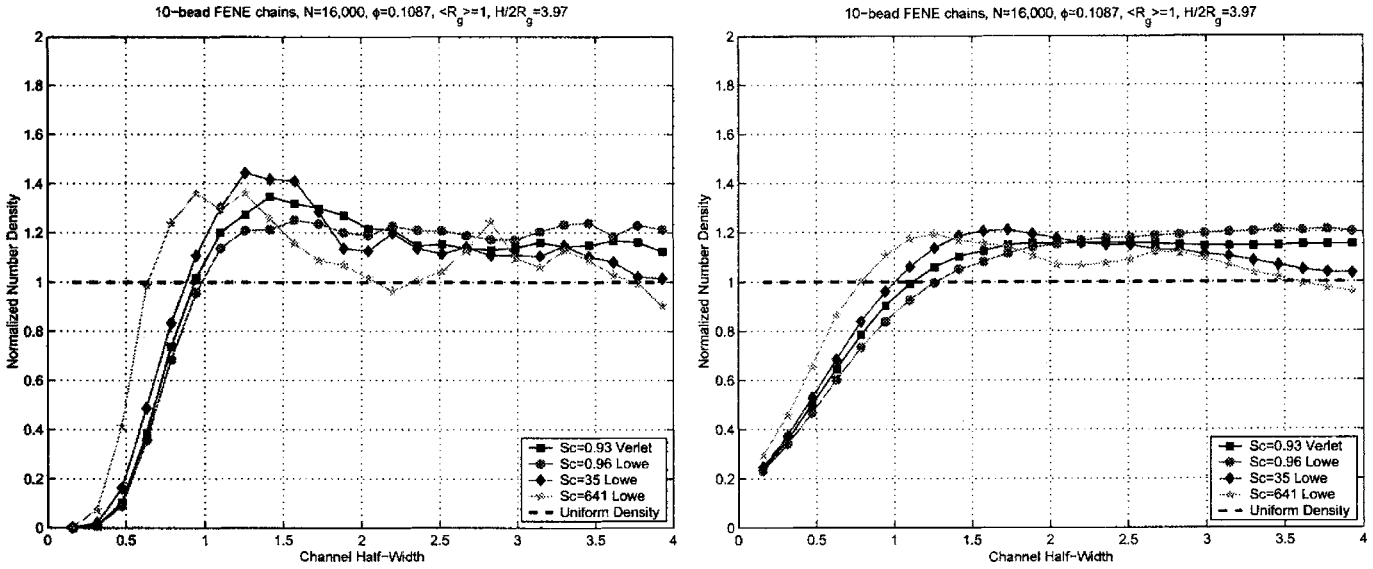

FIG. 8. Normalized polymer number density for ten-bead chains as a function of the distance from the wall for the chain center of mass (left) and beads belonging to chains (right).

on the depletion layer, for the two extreme cases of the Verlet fluid ($S_c \sim 0.96$) and the Lowe fluid ($S_c \sim 642$).

The depletion layer thickness close to wall boundaries can be partially thought to be a result of the internal stresses of the flow, but also a direct consequence of the presence of walls and their effect on the solvent and bead particles through collision. The comparison of the periodic and bounce-forward boundary conditions (Fig. 11) shows that for low Schmidt number regimes ($S_c \sim 1$) the internal stresses of the flow govern the depletion layer thickness, while for high ones ($S_c \sim 642$) the presence of walls has an increasingly stronger effect. Figure 12 indeed depicts a small effect of the boundary conditions in the normalized polymer number density for the Verlet fluid of $S_c \sim 0.96$ as a function of the distance from the wall. When contrasted with the Lowe fluid ($S_c \sim 642$), however, the confinement of the solvent DPD particles seems to have a dominant role in higher S_c regimes. Figure 13 shows a clear effect of the implemented bounce-forward boundary condition on both the chain center-of-mass (left) bead (right) concentration profiles.

X. BULK AND APPARENT WALL VISCOSITY

Viscosities are usually derived from stresses calculated from numerical schemes or from experimental data. For polymer solutions the basic assumption in this process is the spatially homogeneous distribution of the polymer. If depletion layers exist, they are treated as a slip phenomenon. The velocity profiles calculated here are continuous across the channel and display no evidence of slip flow, even though a depletion layer is clearly evident. We have found that the wall shear stress, divided by the wall shear rate is *not* the

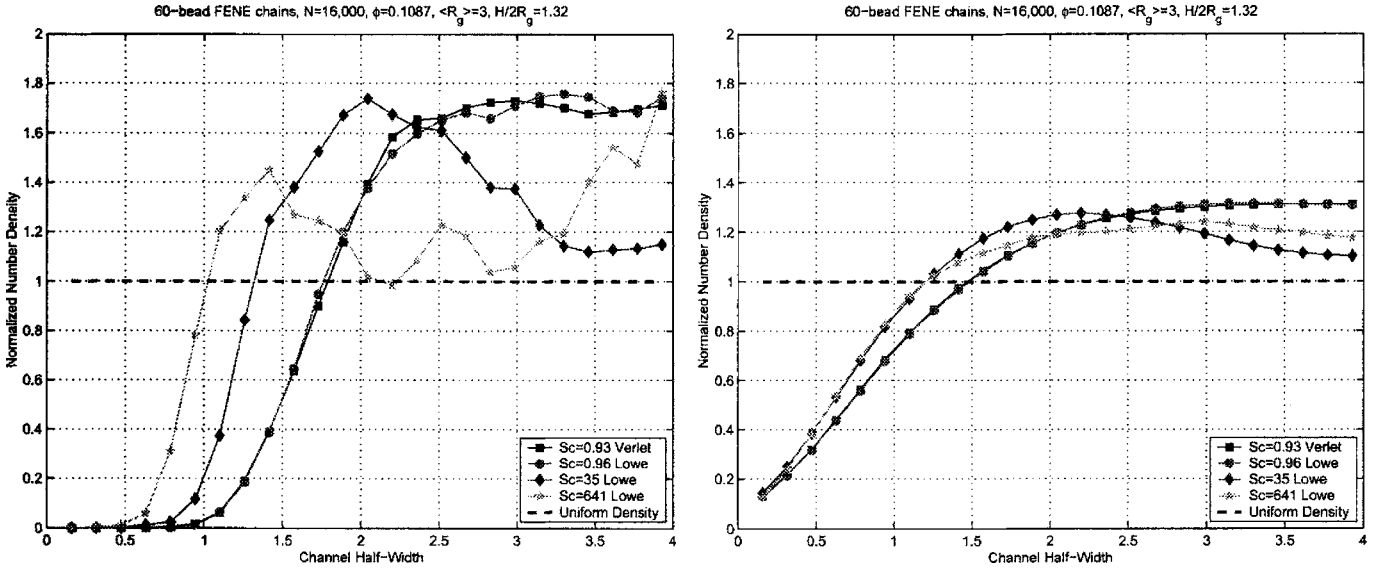

FIG. 9. Normalized polymer number density for 60-bead chains as a function of the distance from the wall for the chain center of mass (left) and beads belonging to chains (right).

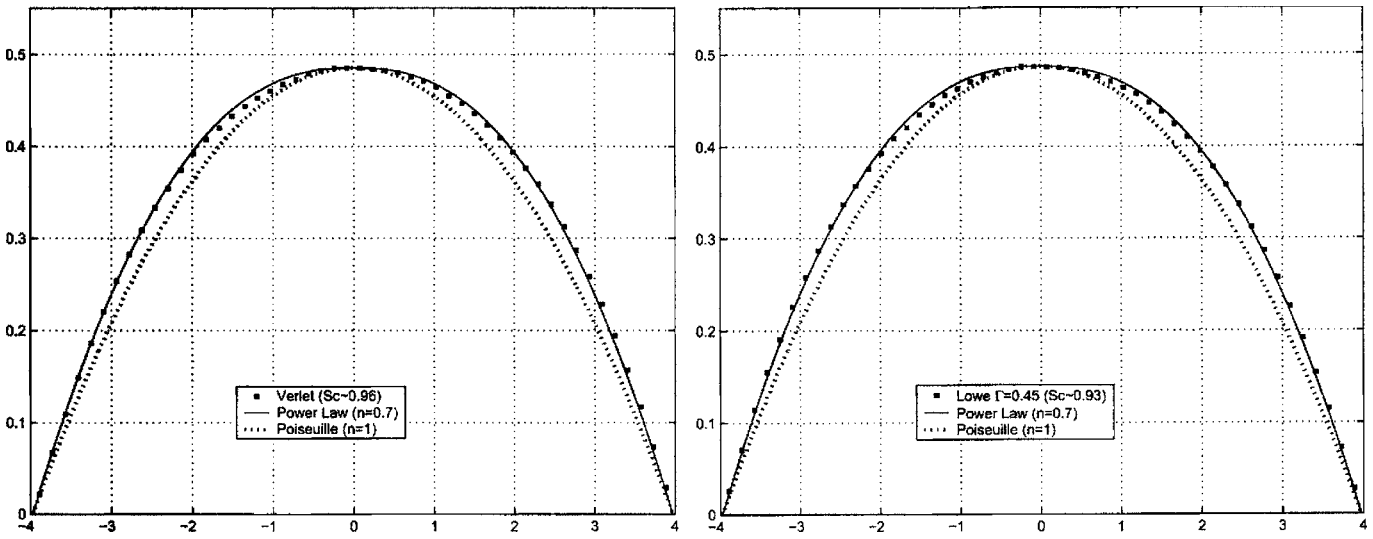

FIG. 10. Velocity profile of 60-bead chain suspension for the velocity-Verlet ($\sigma=3$, left) and Lowe ($\Gamma=0.45$, right) fluids.

same as the bulk viscosity calculated at the same shear rate from plane Couette flow, where no depletion layer is evident. This suggests that Poiseuille flow in microchannels may not be a useful flow for the measurement of viscosity.

We define the viscosity for Couette and for Poiseuille flow as

$$\eta_{\text{bulk}} = \frac{S_{xy}}{\dot{\gamma}}, \quad \eta_{\text{app}} = \frac{\tau_w}{\dot{\gamma}_w},$$

respectively, where S_{xy} is the xy component of the shear stress under steady shear, $\dot{\gamma}=U/L_y$ the shear rate under steady shear, τ_w the wall shear stress in Poiseuille flow, and $\dot{\gamma}_w$ the wall shear rate (i.e., the slope of the tangent of the power law profile) in Poiseuille flow. The Poiseuille driving force g_x can be expressed in terms of the wall shear stress τ_w by a balance of forces as

$$\frac{dP}{dx} = g_x = \frac{2\tau_w}{H}.$$

The simulations were performed in a square box of length 15.874 in each direction and a particle density of $\rho=4$. Table III shows viscosities relative to the solvent values for two fluids: vV at $S_c=0.96$ and for Lowe at $S_c=642$. The high S_c case yields $\eta_{\text{app}} < \eta_{\text{bulk}}$, as expected for the depletion layer. For the low S_c case the relative values are inverted, which is counterintuitive for the depletion layer.

XI. SUMMARY AND DISCUSSION

This paper has presented results for dilute solutions of polymer chains which compare the vV and the Lowe DPD schemes with particular attention to the effect of the self-diffusion Schmidt number of the solvent DPD particles. It was shown that S_c values up to 10^5 are easily attainable with Lowe's method whereas values greater than $\mathcal{O}(1)$ are not

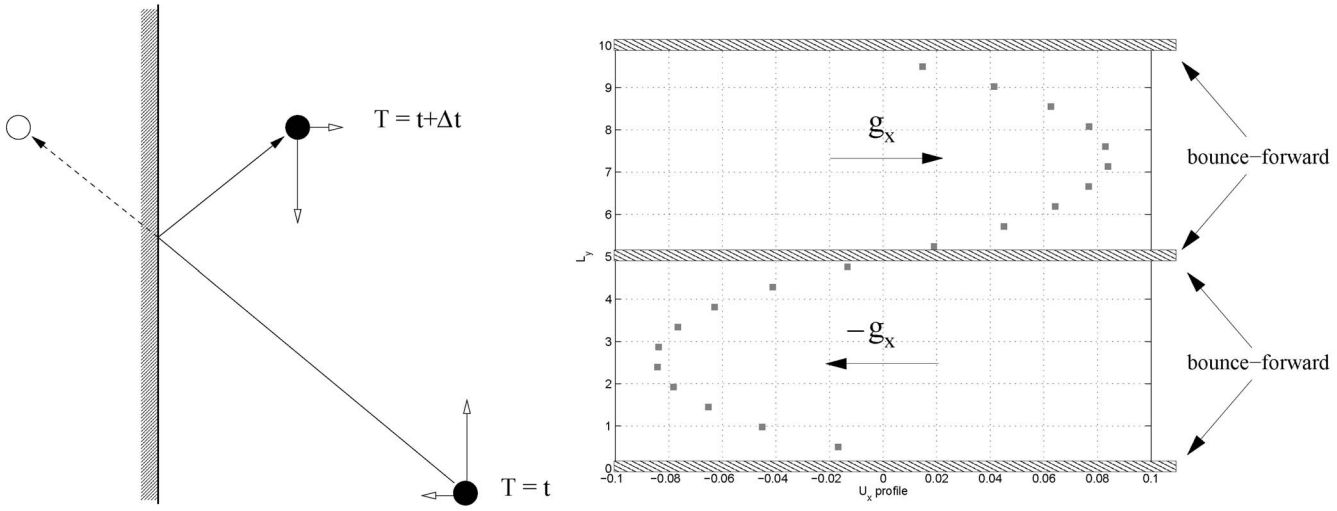

FIG. 11. The bounce-forward boundary condition (Ref. 30) (left) as applied to the periodic Poiseuille profile (right).

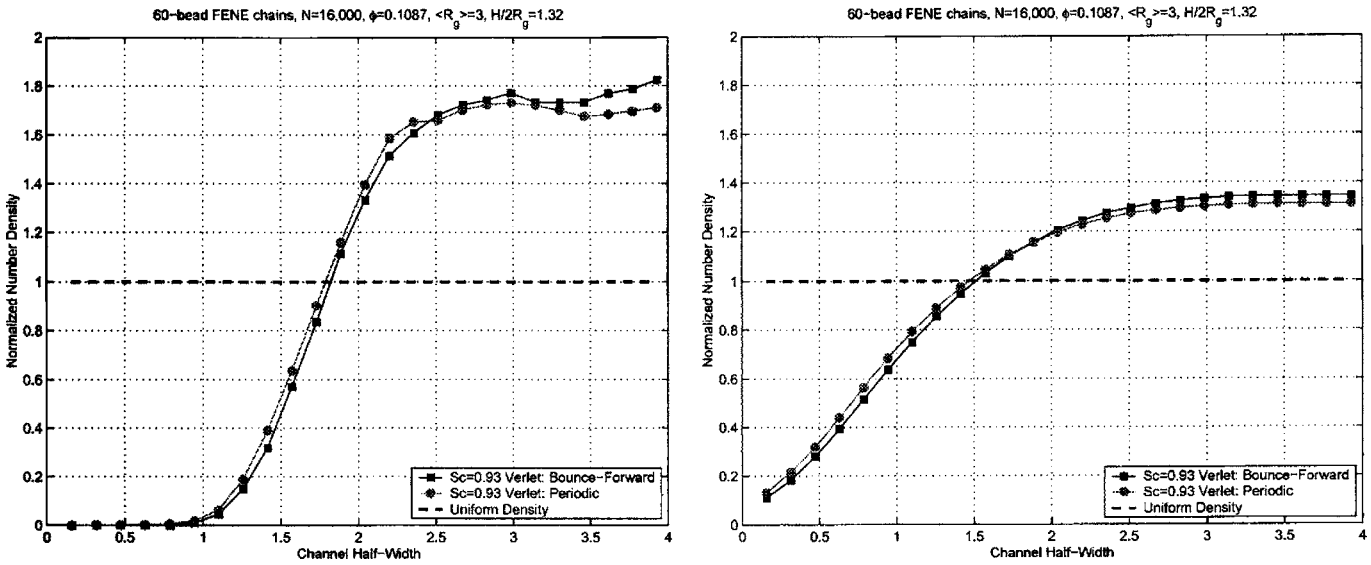

FIG. 12. Verlet fluid ($S_c \sim 0.96$): Bounce-forward boundary condition effect on the normalized polymer number density for 60-bead chains, for the chain center of mass (left) and beads belonging to chains (right).

feasible for the vV scheme. From the calculated viscosity and self-diffusion coefficients, the Stokes-Einstein radius a of a solvent DPD particle was calculated and was found to be $<r_c/4$ for Lowe's scheme (Fig. 5). The assignment of a as the size of a DPD particle is plausible since the total volume of interacting particles of this size is much less than the volume of the sphere of radius r_c. The Reynolds number, defined in the introduction, was calculated for the shear rates driving the fractional extension of the wormlike chain (Fig. 6). Beyond S_c of 500 the calculated extensions change only slightly, and are in good agreement with the experimental data for single λ-DNA molecules. This saturation with respect to S_c together with the decreasing R_e values suggests that the hydrodynamics of the solvent is approaching the Stokes regime. The experimental solvent is a complex buffer solution with sucrose added to enhance its viscosity. Its effective "self-diffusion" coefficient is unknown and appears to have no significance in the analysis of the extension data. This is supported by the successful Brownian dynamics treatment of the same problem[7] in which the solvent is taken to be a homogeneous Newtonian fluid. Chains of 5–60 beads in dilute solution were subjected to Poiseuille flow in microchannels (gap width of a few R_g), and a wall depletion layer of $\mathcal{O}(R_g)$ was observed to form (Figs. 7–9). In each case the layer thickness diminished as S_c was increased to the values which gave the best agreement with the extension data of Fig. 6, the effect being most pronounced for the longer chains. The velocity profiles for these flows (Fig. 10) do not suggest the usual association of depletion layers with slip flow. The profiles are well represented by simple power laws over most of the domain, except for a small parabolic region near the center line. This result suggests that flow curves (pressure loss versus flow rate) measured for dilute polymer solutions in Poiseuille flow do not have a simple interpreta-

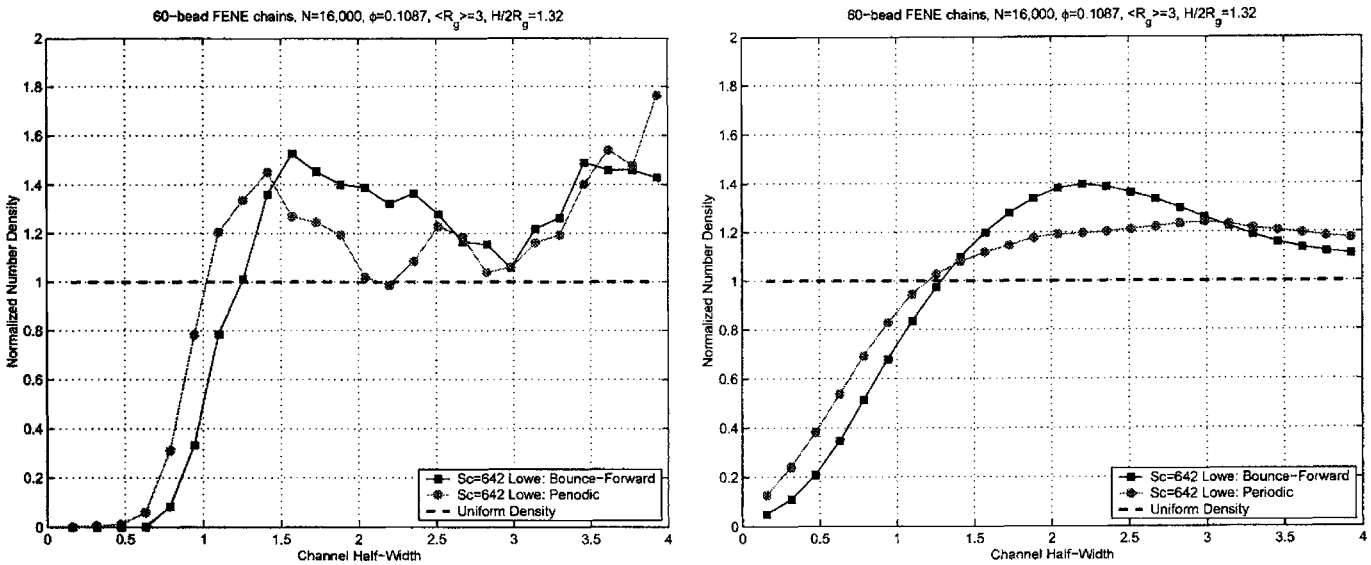

FIG. 13. Lowe fluid ($S_c \sim 642$): Bounce-forward boundary condition effect on the normalized polymer number density for 60-bead chains, for the chain center of mass (left) and beads belonging to chains (right).

TABLE III. Comparison of apparent and bulk viscosities for low and high Schmidt number solvents.

Scheme	η_{solv}	$\dot{\gamma}_w$ (wall)	η_{app}/η_{solv}	S_{xy} (Couette)	η_{bulk}/η_{solv}
vV ($S_c \sim 0.96$)	0.3	0.2973	1.8	0.1111	1.2
Lowe ($S_c \sim 642$)	9.0	0.3055	2.0	10.1235	3.7

tion through the Rabinowitsch[29] equation even with a wall-slip boundary condition. The wall strain rate, calculated from the power law fits, and the imposed wall shear stress together yield apparent wall viscosities which are compared to bulk viscosities obtained from plane Couette flow with uniform concentration (Table III). The absence of chains in the depletion layer suggests that the wall viscosity should be smaller than the bulk value. For large S_c this expectation is fulfilled whereas for $S_c \sim \mathcal{O}(1)$ the relation is inverted, and once again the solvent self-diffusion S_c appears to play a crucial role in dynamic DPD computations.

ACKNOWLEDGMENT

The authors would like to thank the NSF-IMAG program.

[1] R. D. Groot and P. B. Warren, J. Chem. Phys. **107**, 4423 (1997).
[2] C. Marsh, Ph.D. thesis, University of Oxford, 1998.
[3] C. Marsh, G. Backx, and M. Ernst, Phys. Rev. E **56**, 1676 (1997).
[4] C. P. Lowe, Europhys. Lett. **47**, 145 (1999).
[5] H. C. Andersen, J. Chem. Phys. **72**, 2384 (1980).
[6] V. Symeonidis, G. Karniadakis, and B. Caswell, Bull. Pol. Acad. Sci.: Tech. Sci. **53**, 395 (2005).
[7] R. M. Jendrejack, J. J. de Pablc, and M. D. Graham, J. Chem. Phys. **116**, 7752 (2002).
[8] J. S. Hur, E. S. G. Shaqfeh, and R. G. Larson, J. Rheol. **44**, 713 (2000).
[9] E. Peters, Europhys. Lett. **66**, 311 (2004).
[10] V. Symeonidis, G. Karniadakis, and B. Caswell, Phys. Rev. Lett. **95**, 076001 (2005).
[11] J. C. M. Li and P. Chang, J. Chem. Phys. **23**, 518 (1955).
[12] I. Pagonabarraga, M. H. J. Hagen, and D. Frenkel, Europhys. Lett. **42**, 377 (1998).
[13] B. M. Forrest and U. W. Suter, J. Chem. Phys. **102**, 7256 (1995).
[14] P. Español and P. Warren, Europhys. Lett. **30**, 191 (1995).
[15] P. Nikunen, M. Karttunen, and I. Vattulainen, Comput. Phys. Commun. **153**, 407 (2003).
[16] A. Jakobsen, O. Mouritsen, and G. Besold, J. Chem. Phys. **122**, 204901 (2005).
[17] O. Kratky and G. Porod, Recl. Trav. Chim. Pays-Bas **68**, 1106 (1949).
[18] H. Yamakawa, *Modern Theory of Polymer Solutions* (Harper & Row, New York, 1971).
[19] S. F. Sun, *Physical Chemistry of Macromolecules* (Wiley, New York, 1994).
[20] J. F. Marko and E. D. Siggia, Macromolecules **28**, 8759 (1995).
[21] R. G. Larson, T. T. Perkins, D. E. Smith, and S. Chu, Phys. Rev. E **55**, 1794 (1997).
[22] P. T. Underhill and P. S. Doyle, J. Non-Newtonian Fluid Mech. **122**, 3 (2004).
[23] J. Irving and J. Kirkwood, J. Chem. Phys. **18**, 817 (1950).
[24] J. A. Backer, C. P. Lowe, H. C. J. Hoefsloot, and P. D. Iedema, J. Chem. Phys. **122**, 154503 (2005).
[25] D. E. Smith, H. P. Babcock, and S. Chu, Science **283**, 1724 (1999).
[26] C. Bouchiat, M. D. Wang, J.-F. Allemand, T. Strick, S. M. Block, and V. Croquette, Biophys. J. **76**, 409 (1999).
[27] A. W. Lees and S. F. Edwards, J. Phys. C **5**, 1921 (1972).
[28] G. Pan and C. Manke, J. Rheol. **46**, 1221 (2002).
[29] B. Rabinowitsch, Z. Phys. Chem. Abt. A **145**, 1 (1929).
[30] D. C. Visser, H. C. J. Hoefsloot, and P. D. Iedema, J. Comput. Phys. **205**, 626 (2005).